

# Pedestrian trajectory estimation based on foot-mounted inertial navigation system for multistory buildings in post-processing mode

Xiaoji Niu, Tao Liu, Jian Kuang, Quan Zhang, *Member, IEEE*, and Chi Guo, *Member, IEEE*

**Abstract**—Acquiring accurate and reliable pedestrian trajectories is essential for providing indoor location-based services. Although a foot-mounted inertial navigation system (Foot-INS) can acquire pedestrian trajectories in multistory buildings, it will inevitably encounter heading divergence because the constraint information is not always valid. Therefore, we proposed an accurate and convenient post-processing indoor pedestrian positioning system (IPPS) to acquire pedestrian trajectories in multistory buildings such as shopping malls. Based on the hypotheses that the start and end points of the pedestrian trajectories on a single floor were closed, and the horizontal position of the closing point on each floor was identical. Therefore, in the single floor of multistory buildings, we use the closing point to control the trajectory drift error caused by the Foot-INS, and use a smoothing algorithm to reasonably distribute the drift error to the entire trajectory. Heading divergence is unavoidable with the Foot-INS, result in the pedestrian trajectories acquired on different floors were rotationally offset. Because pedestrian trajectories can epitomize the building orientation and provide an opportunity to align those trajectories on multistory buildings, an algorithm was proposed to match the trajectories acquired on different floors. A hybrid simulation experiment was conducted using an accurate reference object to evaluate the positioning performance of the proposed IPPS. The effectiveness of acquiring pedestrian trajectories was also confirmed by various experimental tests in a large shopping mall. The study findings suggest that the proposed IPPS is self-contained, low-cost, and has the potential for large-scale applications.

**Index Terms**—Indoor pedestrian positioning system (IPPS), multistory building, foot-mounted inertial navigation system (Foot-INS), trajectory matching.

## I. INTRODUCTION

THE growing requirement for providing indoor location-based services (ILBS) demands the acquisition of precise and reliable location information. In fact, the global indoor navigation and positioning market is predicted to reach 17 billion USD in 2025 [1]. Pedestrian trajectories can play a critical role in ILBS, such as by helping to quickly analyze users' behaviors and establish wireless fidelity (WiFi) fingerprint

databases in shopping malls. Toward those goals, academia and industry are both developing promotable straightforward indoor pedestrian positioning systems (IPPSs) to reliably and accurately determine people's trajectories in unmapped indoor buildings. Currently, IPPSs are categorized as either wireless-positioning or sensor-based solutions. Wireless positioning mainly includes WiFi [2, 3], Bluetooth low energy (BLE) [4], ZigBee [5], radio-frequency identification (RFID) tags [6], acoustic [7], and ultrawideband (UWB) [8]. Regardless of whether geometric-based (e.g., time-difference-of-arrival) or received signal strength fingerprinting based positioning methods are used, communications infrastructure must be pre-installed in facilities to support wireless positioning. Although WiFi technology can benefit from the existing communications infrastructure and avoid tedious on-site manual installation, calibrating and measuring the infrastructure requires the support of other positioning technologies or the use of professional measurement instruments. Moreover, when a fire, power failure, or other emergency or accident occurs, wireless positioning systems will be impacted, and their reliability will be drastically reduced. On the contrary, sensor-based positioning systems do not require any infrastructure support and are more suitable for application to unmapped indoor environments.

Sensor-based indoor positioning systems can be categorized as magnetic-field positioning, simultaneous localization and mapping (SLAM), and inertial sensor based dead-reckoning (DR). According to one hypothesis, indoor magnetic fields are non-uniform, and their fluctuations are rooted in the natural geographic distribution and in various permanent artificial structures (e.g., reinforced concrete structures). Therefore, magnetic anomalies can be used as fingerprints for indoor positioning [9, 10]. However, magnetic-field positioning is exceptionally susceptible to environmental changes such as the magnetic-field variations arising from the rearrangement of shop layouts. Moreover, similar magnetic-field characteristics at different positions can confuse the system. In addition, as with WiFi technology, magnetic-field positioning requires human resources and financial investment to construct and maintain a fingerprint database. In SLAM, pedestrians hold a sensor consisting of, e.g., a red-green-blue-depth imaging camera and a three-dimensional laser scanner, to collect surrounding environmental information, build a map of an unknown indoor environment, and localize the pedestrian in the map [11, 12]. However, in nearly homogeneous indoor environments such as long and narrow corridors consisting of

Manuscript received May 7, 2021; revised XX XX, 202X; accepted XX XX, 20XX. Date of publication XX XX, 20XX. This work was supported by the National Key Research and Development Program of China under Grant 2018YFC0809804, Grant 2016YFB0502202 and Grant 2016YFB0501803. (Corresponding author: Jian Kuang.)

X. Niu, T. Liu, J. Kuang, Q. Zhang and C. Guo are with the GNSS Research Center, Wuhan University, Wuhan, Hubei, CO 430072 PR China. X. Niu and Q. Zhang are also with the Collaborative Innovation Center of Geospatial Technology, Wuhan University. C. Guo is also with the Artificial Intelligence Institute, Wuhan University. (E-mails: xjniu@whu.edu.cn; liu\_tao@whu.edu.cn; kuang@whu.edu.cn; zhangquan@whu.edu.cn; guochi@whu.edu.cn).

only walls and a floor, the camera and laser-scanner sensors can be “blinded.” Moreover, changes in lighting conditions can also reduce the camera effectiveness. In inertial sensor-based DR systems, wearable inertial sensors (contain at least three-axis gyroscopes and accelerometers) are used to locate a pedestrian’s position by orientation projection and numerical integration [13–16]. Because it is completely independent of any external signal or facilities and has short-term high-precision highlights, inertial-sensor-based DR has attracted the attention of many researchers.

Advances in micro-electro-mechanical systems (MEMS) technology has promoted the continuous development of MEMS inertial measurement units (IMU) toward miniaturization, high performance, low cost, and low power consumption. MEMS IMU can be attached to the human body as a wearable device and has been widely used in pedestrian navigation systems [17]. Fundamentally, inertial sensor-based IPPS usually include pedestrian dead reckoning (PDR) and inertial navigation system (INS) algorithms [18]. Compared with the PDR algorithm, the INS-based system is not limited by different motion modes and does not require the parameters to be optimized to adapt to different pedestrians. Foot mounted INS (Foot-INS) is the most well-known INS-based pedestrian positioning system wherein a MEMS IMU is attached on foot to locate a pedestrian. However, the angular rate and specific force data measured by IMU contain biases and other sensor errors, result in the positioning error exponentially accumulate over time, which is more evident in low-quality MEMS IMU [19, 20]. Therefore, Foxlin [21] proposed the zero velocity update (ZUPT) algorithm to mitigate the accumulated error in Foot-INS. Since then, ZUPT as an essential algorithm and has been widely used in Foot-INS. Pedestrian walking can be considered as the movement of foot alternately conversion between swing and stance phases. During the stance phase, the foot is stationary, and its ideal velocity is zero. Once the stance phase is correctly detected, the zero velocity can be used as independent observation information to correct the navigation error of Foot-INS via a Kalman filter (KF). ZUPT algorithm can significantly decrease the divergence speed of the positioning error, and its positioning performance is usually better than 5% of the travel distance.

The heading error and z-axis gyro bias of the ZUPT algorithm are unobservable from zero velocity measurement, which causes the positioning error of the system to still diverge over time [22, 23]. Therefore, most current Foot-INS research is focused on improving the observability of the system’s heading error or z-axis gyro bias. The zero angular rate update (ZARU) algorithm has been proposed to estimate the gyroscope bias [13, 22]. This approach assumed that the IMU attitude is constant and that its measured angular rate is theoretically zero when the IMU is stationary. However, the ZARU algorithm must be adapted to rigorous stationary conditions. During walking, the pedestrian’s foot is not entirely static but is accompanied by slightly jittery in each stance phase. Therefore, the conditions of the ZARU algorithm are only satisfied when the pedestrian is stationary for a long time. Because the corridors in most indoor buildings (especially office buildings) are straight, parallel,

or mutually orthogonal, the corridors determine the dominant building directions. When pedestrians walk along a straight line parallel to the dominant direction, the heuristic drift elimination (HDE) algorithm can be used to estimate the gyro bias [24]. An improved HDE (iHDE) algorithm was developed to adapt to situations where pedestrians walk in straight lines but not parallel to the building’s dominant directions [25]. Both HDE and iHDE methods are a kind of straight-line constraint algorithms. The straight-line constraint algorithm will encounter Waterloo when some indoor buildings’ passable paths are neither straight nor mutually orthogonal, such as many curved paths in shopping malls. Some researchers have proposed using magnetometers to overcome the unobservable heading error in Foot-INS [15, 16]. Magnetometers are usually integrated with inertial sensors and attached to the foot (near the floor). However, numerous ferromagnetic materials are used in indoor building structures (e.g., floors), which can cause magnetic interference. These interferences will increase the unreliability of the magnetometer, resulting in significant positioning errors. Deng *et al.* [26] proposed a body odometer (BOR) model to assist Foot-INS, and used a complementary filter and an HDE algorithm to mitigate the gyro bias and improve the heading estimation accuracy. However, the BOR model demands training appropriate parameters to match different people and various walking patterns, which limits the widespread application of this approach. In our previous work [27, 28], we used sparse control points to improve the observability of the heading error in Foot-INS, thereby improving positioning accuracy. However, measuring control point coordinates requires the support of professional surveying equipment, which is very unfriendly for general indoor positioning applications, especially those used in multistory buildings (e.g., shopping malls).

The indoor map matching-based Foot-INS method can effectively suppress the position errors accumulation and estimate the heading angle. It is a classic post-processing method for the pedestrian positioning system [29–31]. This method uses the following observations of an indoor map: pedestrian trajectories are restricted by buildings (e.g., the pedestrian cannot walk through walls and atrium areas of shopping malls), or the relatively unchanged position information of crucial structures (e.g., the relative positions between the entrance and escalators). A particle filter is usually used to achieve information fusion between the Foot-INS and the map observations. Map matching-based methods require prior map information, and the positioning performance is determined by the map observations accuracy. In practical applications, the map matching-based method is unsuitable for large-scale applications because it is challenging to obtain indoor maps of multiple multistory buildings in a large-scale area (e.g., all shopping malls in a city or a province). The indoor map construction requires a vast material and human resources investment, and it encounters some non-technical challenges, such as the unwillingness of businesses to cooperate.

Multistory buildings can significantly increase land utilization and are an essential component of urban development. Typical multistory buildings include residential buildings, shopping malls, office buildings, and hospitals. Elevators can

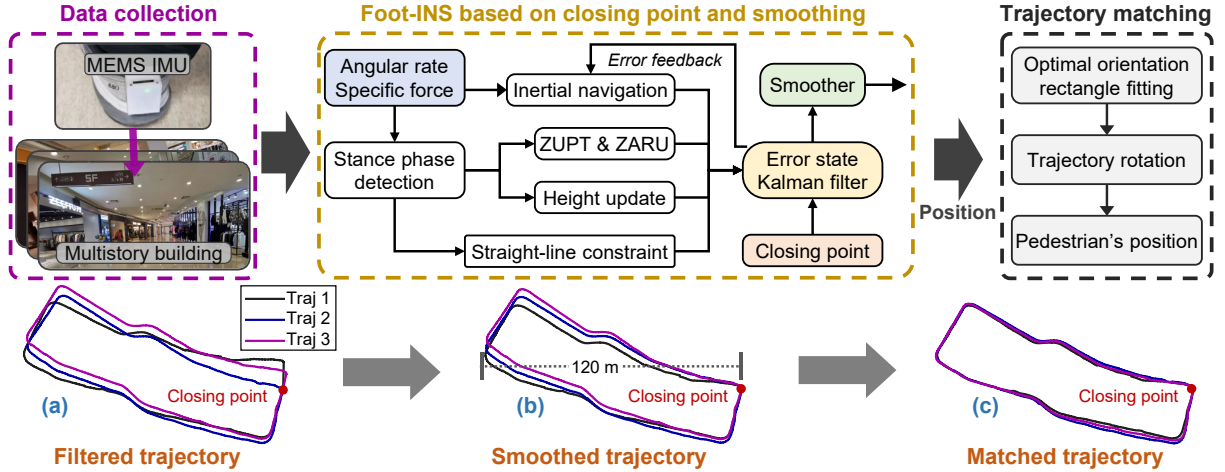


Fig. 1. Proposed IPSS for application to multistory buildings. Top diagram provides overview of the proposed IPSS, and lower figures (a-c) show an example of proposed IPSS when tester walks three times along a similar route on one floor in a shopping mall.

facilitate people’s daily life and are indispensable in multistory buildings. Toward the goals of life preservation and public safety, fire-fighting stairs are also indispensable for evacuating people and supporting rescue efforts in emergencies (e.g., fires and earthquakes) [32]. In fact, the horizontal positions of fire-fighting stairs and elevators on all the floors of almost all multistory buildings are identical regardless of each floor’s internal layout, which is useful information for developing an accurately and reliably IPSS.

In this paper, we present an IPSS based on Foot-INS and the multistory building’s inherent structural characteristics in post-processing mode, so as to accurately and reliably estimate pedestrian trajectories in a multistory building. We used the ZUPT, ZARU, straight-line constraint, and height update algorithms to improve the autonomous positioning ability of the Foot-INS. A fire-fighting stair or elevator in a multistory building was selected as the closing point in our system to increase the pedestrian-position accuracy and reliability of the Foot-INS. Moreover, a smoothing algorithm was used to increase the estimation accuracy of the pedestrian trajectory. However, because the system heading divergence was unavoidable, the estimated pedestrian trajectories were rotationally offset on different floors. Therefore, we propose a trajectory matching algorithm to correct the rotational offset problem. The proposed IPSS is self-contained and does not require surveying the building in advance, nor does it require any external equipment support. Furthermore, because the IPSS does not require testers to have a professional background, it shows excellent scalability and potential for large-scale promotion. The proposed system has the potential to promote a wide range of indoor positioning technology practical application and implementation.

The remainder of the paper is organized as follows. An overview of the proposed system is provided in Section II. Section III describes the Foot-INS based on closing point and smoothing algorithm. In Section IV, a trajectory matching algorithm is proposed. Section V presents the experimental results. Section VI summarizes the key study findings and proposes a direction for future work.

## II. SYSTEM OVERVIEW

As shown in Fig. 1, the data were acquired using the proposed Foot-INS-based IPSS, refined using the closing points and smoothing algorithm, and rotationally corrected using the trajectory matching algorithm. Before the data collection, a compact inertial module was tightly attached to the heel of a pedestrian’s shoe. The inertial module was comprised of a low-cost MEMS IMU, a power supply module, a low-energy Bluetooth module, a data storage module, and a general multi-protocol system-on-chip. Based on the previous compact inertial module [28], we enhanced the module’s adaptability under different environmental temperatures and optimized the power supply to support longer-term positioning applications. The main technical characteristics of the inertial module are given in Table I.

TABLE I  
MAIN CHARACTERISTICS OF THE MEMS INERTIAL MODULE

| Parameters       | Gyroscope                              | Accelerometer                      |
|------------------|--|------------------------------------|
| Data rate        | 200 Hz                                 | 200 Hz                             |
| Dynamic range    | 2000 °/s                               | 16 g                               |
| Bias instability | 10 °/h                                 | 0.2 mg                             |
| White noise      | $0.24 \text{ } ^\circ/\sqrt{\text{h}}$ | $0.06 \text{ m/s}/\sqrt{\text{h}}$ |
| Weight           | $\approx 50 \text{ g}$                 |                                    |
| Size (no shell)  | $32 \times 25 \times 12 \text{ mm}$    |                                    |
| Battery power    | continuous work for more than 10 hours |                                    |

During the data collection, the tester had to install a simple smartphone application to control the inertial module’s start and end, and Fig. 2 presents a sample screenshot of the smartphone application. Furthermore, when the tester arrived at a fire-fighting stair or elevator (also named as a closing point in this paper) in the multistory building, the application sent an identifier to the inertial module to facilitate the subsequent offline data processing. The tester was required to walk at least one closed path and back to the closing point on each floor, and then follow the stairs to reach the next floor. That is, the start and end points of the pedestrians walking on a single floor coincided. Overall, the tester only had to walk normally and as

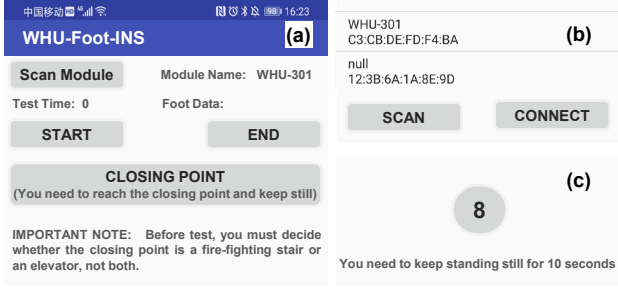


Fig. 2. Screenshot of application showing sample of data acquired using proposed IPPS. (a) Main application screenshot. (b) and (c) Screenshots of “scan module” and “closing point” buttons, respectively.

straight as possible (although not mandatory), and then simply push a few buttons in the smartphone application to complete the test. Moreover, because the tester does not require any relevant professional knowledge, the system is feasible and highly user-friendly for practical applications.

It should be noted that the closing point in the proposed system is recognized by manually sending a command rather than automatically. In practical applications, the closing point can be automatically identified from the IMU data. For example, in an elevator scene, the objective acceleration and deceleration movement can be detected from the measured specific force data, thereby automatically identifying the closing point. Even if the selected closing points are different, the matched trajectories of different floors are consistent, i.e., the obtained relative trajectories of different floors in a multistory building are accurate.

Fire-fighting stairs and elevators are indispensable components in multistory buildings, and the elevator is the most used cross-floor tool. Therefore, the fire-fighting stair or elevator is determined as the closing point of the proposed system. The horizontal position of the closing point of each floor is the same. As shown in the yellow-dashed box in Fig. 1, on each floor of multistory buildings, we used the closing point to improve the accuracy and reliability of Foot-INS. A smoothing algorithm is used to obtain a higher precision pedestrian trajectory in the proposed IPPS. However, because the heading error could not be effectively estimated using the closing point, the pedestrian trajectories were rotationally offset on different floors. Therefore, as shown in the black-dashed box in Fig. 1, we propose a trajectory matching algorithm to correct for the rotational offset problem during data post-processing.

### III. FOOT-INS WITH CLOSING POINT AND SMOOTHING

In this section, we leverage the closing points of the multistory building to correct the Foot-INS. The inertial navigation algorithm and stance phase detection method are introduced first. Then, we describe the system state and measurement models in detail. Finally, a smoothing algorithm is used to further improve the trajectory estimation accuracy.

#### A. Inertial Navigation Algorithm

The navigation coordinate frame (i.e.,  $n$  frame) is defined using the famous North-East-Down (NED) geographic coordinate system. The typical body coordinate frame (i.e.,  $b$

frame) is adopted, wherein the coordinate origin is at the geometric center of the IMU, and  $x$ ,  $y$ , and  $z$  represent the forward, right, and down axes, respectively. The inertial navigation algorithm integrates the angular rate and specific force measured by the IMU to calculate the attitude, velocity, and position of the foot [33]. Because the data acquired using the low-quality gyroscopes in MEMS IMU are considerably noisy, it is difficult to separate Earth’s rotation from the angular rate. Therefore, we neglect Earth’s rotation components in the inertial navigation algorithm [34]. Knowing the precise attitude calculation is important, and it is computed from the attitude quaternion updating equation as follows:

$$\mathbf{q}_{b,k}^n = \mathbf{q}_{b,k-1}^n \otimes \left[ \cos \|0.5\boldsymbol{\phi}_k\| \frac{\sin \|0.5\boldsymbol{\phi}_k\|}{\|\boldsymbol{\phi}_k\|} (\boldsymbol{\phi}_k)^T \right]^T \quad (1)$$

$$\boldsymbol{\phi}_k \approx \boldsymbol{\alpha}_k + \frac{1}{12} \boldsymbol{\alpha}_{k-1} \times \boldsymbol{\alpha}_k \quad (2)$$

where  $\otimes$  is quaternion product operator;  $\|\cdot\|$  and  $(\cdot)^T$  represent the magnitude and transposition function, respectively;  $\mathbf{q}_{b,k}^n$  is the attitude quaternion relating the  $b$  frame to the  $n$  frame at time  $t_k$ ;  $\boldsymbol{\alpha}_k \approx \boldsymbol{\omega}_k^b \Delta t$ , with  $\boldsymbol{\omega}_k^b$  being the perceived angular rate; and  $\Delta t$  is the sampling interval. The corresponding attitude matrix  $\mathbf{C}_b^n$  can be obtained from the quaternion  $\mathbf{q}_b^n = [q_1 \ q_2 \ q_3 \ q_4]^T$  as follows:

$$\mathbf{C}_b^n = \begin{bmatrix} q_1^2 + q_2^2 - q_3^2 - q_4^2 & 2(q_2q_3 - q_1q_4) & 2(q_2q_4 + q_1q_3) \\ 2(q_2q_3 + q_1q_4) & q_1^2 - q_2^2 + q_3^2 - q_4^2 & 2(q_3q_4 - q_1q_2) \\ 2(q_2q_4 - q_1q_3) & 2(q_3q_4 + q_1q_2) & q_1^2 - q_2^2 - q_3^2 + q_4^2 \end{bmatrix} \quad (3)$$

From the updated attitude matrix  $\mathbf{C}_b^n$  and the measured specific force  $\mathbf{f}^b$ , the current velocity  $\mathbf{v}_k^n$  and position  $\mathbf{r}_k^n$  can be updated as follows:

$$\mathbf{v}_k^n = \mathbf{v}_{k-1}^n + \int_{t_{k-1}}^{t_k} \mathbf{C}_b^n \mathbf{f}^b dt + \mathbf{g}^n \Delta t \quad (4)$$

$$\mathbf{r}_k^n = \mathbf{r}_{k-1}^n + 0.5 (\mathbf{v}_{k-1}^n + \mathbf{v}_k^n) \Delta t \quad (5)$$

where  $\mathbf{g}^n = [0 \ 0 \ g]^T$  and  $g$  is the gravitational acceleration.

In the proposed IPPS, the tester needs to stand and remains stationary for a few seconds before walking at the beginning. The specific force measured by the accelerometers corresponds to the local gravity with respect to the sensor body frame. Thus, the initial roll and pitch angle can be calculated by the gravity constraint [15, 27]. Moreover, the initial position and heading angle were set to zero.

#### B. Stance Phase Detection

Human walking can be thought of as a periodic and repetitive movement consisting of one gait cycle after another, and one gait cycle can be subdivided into stance and swing phases [35, 36]. During the stance phase, the velocity of a pedestrian’s foot is approximately zero, and this material fact is the origin of Foot-INS research. Therefore, having an accurate and reliable stance phase detection algorithm is critical to Foot-INS.

We used the well-known generalized likelihood ratio test (GLRT) approach to detect the stance phase in each gait cycle [35]. When the IMU is stationary, this detection method

assumes that the measured specific force is equivalent to the gravitational acceleration projection on the  $b$  frame and that the measured angular rate is approximately zero. The GLRT principle is given as follows:

$$\lambda_k = \frac{1}{2N+1} \sum_{j=k-N}^{k+N} \left( \frac{1}{\sigma_a^2} \left\| \mathbf{f}_k^b - g \frac{\overline{\mathbf{f}_k}}{\|\overline{\mathbf{f}_k}\|} \right\|^2 + \frac{1}{\sigma_\omega^2} \|\boldsymbol{\omega}_k^b\|^2 \right) \quad (6)$$

$$D_k = \begin{cases} 1, & \text{if } \lambda_k < T_\lambda \\ 0, & \text{others} \end{cases} \quad (7)$$

where  $\lambda_k$  is the detection statistic;  $D_k$  is the stance phase detection output;  $\overline{\mathbf{f}_k}$  is the mean specific force in time interval  $[t_{k-N}, t_{k+N}]$ ;  $\sigma_a^2$  and  $\sigma_\omega^2$  are the specific force and angular rate measurement error standard deviations, respectively;  $N$  is the detection window size and is set to 5; and  $T_\lambda$  is the GLRT detection threshold, which is set to  $0.5 \times 10^5$ .

However, a few detection statistics generated during the stance phase are above the detection threshold, but a few generated during the swing phase are below the detection threshold, both of which will result in failure to detect the stance phase (7) [36]. When a person is walking normally, the gait phase (swing or stance phase) is continuous and duration for a period of time, and this duration time is at least 0.15 s (30 epochs for a 200 Hz sampling frequency). Therefore, we developed a more reliable method of detecting the stance phase based on the GLRT detection output (7), and the proposed detection algorithm is given in Algorithm 1. As shown in Fig. 3, the proposed approach can effectively improve the stance phase detection's reliability and accuracy.

---

#### Algorithm 1 Proposed Stance Phase Detection

---

**input:** obtain  $D_k$  by (7), set  $m=31, m_1=5, m_2=0.5(m-1)$

**output:** updated detection output  $D_k$

- 1: STEP1: revise failure detections in stance phase
  - 2: **for**  $k = m_2 + 1, \dots, n - m_2$  **do**
  - 3: get  $N_1 = \min\{D_{k-m_2}, \dots, D_{k-m_2+m_1-1}\}$ ,  $N_2$  (number of elements 1 in set  $\{D_{k-m_2+m_1}, \dots, D_{k+m_2-m_1}\}$ ),  $N_3 = \min\{D_{k+m_2-m_1+1}, \dots, D_{k+m_2}\}$
  - 4: **if**  $N_1 = 1$  and  $N_2 \geq 0.6(m-2m_1)$  and  $N_3 = 1$  **then**
  - 5: reset:  $D_j = 1$  ( $j = k - m_2, \dots, k + m_2$ )
  - 6: **end if**
  - 7: **end for**
  - 8: STEP2: revise failure detections in swing phase
  - 9: get set  $S$ :  $S \subseteq D$ ,  $\min S = 1$ ,  $S$  is continuous and ( $\min\{S, D_{k+1}\} = 0$  or  $k+1 = n$ )
  - 10: **if**  $N_4 < m - 2m_1$  ( $N_4$  is size of set  $S$ ) **then**
  - 11: reset:  $\forall D_i \subseteq S, D_i = 0$
  - 12: **end if**
- 

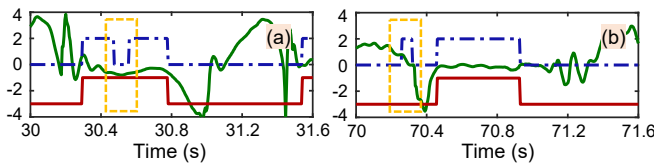


Fig. 3. Stance phase detection results. Green line represents gyro z-axis data (rad/s), blue line is obtained by Eq.(7), and red line represents Algorithm 1 statistics. Yellow boxes in (a) and (b) represent failure detection calculated using Eq. (7) during stance and swing phases, respectively.

#### C. System State Model

Profiting from the efficiency and reliability of the KF [37], we used the KF to fuse the inertial navigation and measurement information. The state vector of the Foot-INS can be defined as follows:

$$\mathbf{X} = [\delta \mathbf{r}^n \quad \delta \mathbf{v}^n \quad \phi \quad \mathbf{b}_a \quad \mathbf{b}_g]^T \quad (8)$$

where  $\delta \mathbf{r}^n$ ,  $\delta \mathbf{v}^n$ ,  $\phi$ ,  $\mathbf{b}_a$ , and  $\mathbf{b}_g$  are the position errors, velocity errors, attitude errors, accelerometer biases, and gyroscope biases, respectively. The gyroscope and accelerometer biases can be regarded as a first-order Markov process. As explained in Section II, Earth's rotational components are neglected. Hence, the continuous system state model is derived as follows:

$$\dot{\mathbf{X}} = \mathbf{F}\mathbf{X} + \mathbf{G}\mathbf{W} \quad (9)$$

$$\left\{ \begin{array}{l} \mathbf{F} = \begin{bmatrix} \mathbf{0}_{3 \times 3} & \mathbf{I}_{3 \times 3} & \mathbf{0}_{3 \times 3} & \mathbf{0}_{3 \times 3} & \mathbf{0}_{3 \times 3} \\ \mathbf{0}_{3 \times 3} & \mathbf{0}_{3 \times 3} & \mathbf{f}^n \times & \mathbf{C}_b^n & \mathbf{0}_{3 \times 3} \\ \mathbf{0}_{3 \times 3} & \mathbf{0}_{3 \times 3} & \mathbf{0}_{3 \times 3} & \mathbf{0}_{3 \times 3} & -\mathbf{C}_b^n \\ \mathbf{0}_{3 \times 3} & \mathbf{0}_{3 \times 3} & \mathbf{0}_{3 \times 3} & -1/\tau_{ba} & \mathbf{0}_{3 \times 3} \\ \mathbf{0}_{3 \times 3} & \mathbf{0}_{3 \times 3} & \mathbf{0}_{3 \times 3} & \mathbf{0}_{3 \times 3} & -1/\tau_{bg} \end{bmatrix} \\ \mathbf{G} = \begin{bmatrix} \mathbf{0}_{3 \times 3} & \mathbf{0}_{3 \times 3} & \mathbf{0}_{3 \times 3} & \mathbf{0}_{3 \times 3} \\ \mathbf{C}_b^n & \mathbf{0}_{3 \times 3} & \mathbf{0}_{3 \times 3} & \mathbf{0}_{3 \times 3} \\ \mathbf{0}_{3 \times 3} & -\mathbf{C}_b^n & \mathbf{0}_{3 \times 3} & \mathbf{0}_{3 \times 3} \\ \mathbf{0}_{3 \times 3} & \mathbf{0}_{3 \times 3} & \mathbf{I}_{3 \times 3} & \mathbf{0}_{3 \times 3} \\ \mathbf{0}_{3 \times 3} & \mathbf{0}_{3 \times 3} & \mathbf{0}_{3 \times 3} & \mathbf{I}_{3 \times 3} \end{bmatrix} \end{array} \right. \quad \mathbf{W} = \begin{bmatrix} \mathbf{w}_a \\ \mathbf{w}_g \\ \mathbf{w}_{ba} \\ \mathbf{w}_{bg} \end{bmatrix} \quad (10)$$

where  $\mathbf{F}$  is the dynamic transform matrix;  $\mathbf{f}^n \times$  is the skew-symmetric matrix of  $\mathbf{f}^n$ ;  $\tau_{ba}$  and  $\tau_{bg}$  are the correlation times, which are set to 1800 s;  $\mathbf{G}$  is the noise distribution matrix; and  $\mathbf{W}$  is the system noise, which is assumed to be zero-mean Gaussian white noise with the correlation covariance matrix  $\mathbf{Q}$ ;  $\mathbf{w}_a$  and  $\mathbf{w}_g$  are the measurement white noises of the accelerometer and gyroscopes, respectively; and  $\mathbf{w}_{ba}$  and  $\mathbf{w}_{bg}$  are the driving white noises of the bias model.

Because the MEMS IMU sampling interval  $\Delta t$  (0.005 s) is very small, and  $\mathbf{F}_k \Delta t \ll \mathbf{I}$ , the discrete-time system state model can be derived as follows:

$$\mathbf{X}_k = \Phi_{k,k-1} \mathbf{X}_{k-1} + \mathbf{w}_{k-1} \quad (11)$$

$$\left\{ \begin{array}{l} \Phi_{k,k-1} = \exp[\mathbf{F}_{k-1} \Delta t] \approx \mathbf{I}_{15 \times 15} + \mathbf{F}_{k-1} \Delta t \\ \mathbf{Q}_k \approx \frac{\Delta t}{2} (\Phi_{k,k-1} \mathbf{G}_{k-1} \mathbf{Q} \mathbf{G}_{k-1}^T \Phi_{k,k-1}^T + \mathbf{G}_k \mathbf{Q} \mathbf{G}_k^T) \end{array} \right. \quad (12)$$

where  $\Phi_{k,k-1}$  is the discrete transform matrix, and  $\mathbf{Q}_k$  is the covariance matrix of the discrete system noise  $\mathbf{w}_{k-1}$ .

#### D. System Measurement Model

Multi-constraint correction algorithms (including the ZUPT, ZARU, straight-line constraint, and height update algorithms) were employed to improve the accuracy and reliability of the Foot-INS. Although the ZUPT algorithm is always effective, the ZARU and straight-line constraint ones do not always work well. For example, the straight-line constraint algorithm is completely ineffective when pedestrians walk along a randomly curved path. We used the height update algorithm to determine the floor where pedestrians were located. Then, we further used immutable closing points (e.g., the fire-fighting

stairs or elevators) in the multistory building to enhance the robustness of the Foot-INS.

1) *Zero Velocity Update (ZUPT)*: Once the stance phase has been correctly detected by Algorithm 1, the zero velocity is an independent observation exhibiting zero mean white noise and can be used to correct the Foot-INS, and the ZUPT model is given as follows:

$$\mathbf{v}_{I,k}^n - \mathbf{0}_{3 \times 1} = [\mathbf{0}_{3 \times 3} \quad \mathbf{I}_{3 \times 3} \quad \mathbf{0}_{3 \times 9}] \mathbf{X}_k + \varepsilon_v \quad (13)$$

where  $\mathbf{v}_{I,k}^n$  is the velocity provided by the inertial navigation algorithm at time  $t_k$ , and measurement noise  $\varepsilon_v$  is the white noise with the covariance matrix  $\mathbf{R} = \text{diag}[(0.03)_{3 \times 1}^2]$ .

2) *Zero Angular Rate Update (ZARU)*: When the IMU is stationary, the theoretical angular rate is zero; therefore, the ZARU model can be derived as follows:

$$\boldsymbol{\omega}_k^b - \mathbf{0}_{3 \times 1} = [\mathbf{0}_{3 \times 12} \quad \mathbf{I}_{3 \times 3}] \mathbf{X}_k + \varepsilon_\omega \quad (14)$$

where  $\varepsilon_\omega$  is the angular rate noise, which is the standard deviation of the angular rate observed in a stationary state. The noise covariance matrix  $\mathbf{R}$  is  $\text{diag}[(1.0^\circ)_{3 \times 1}^2]$ . Because the ZARU algorithm has a more stringent requirement in the stationary condition, we used the judgment strategy shown in Algorithm 2 to commence the ZARU model.

---

#### Algorithm 2 ZARU Judgment Strategy

---

**input:** get detection statistics  $\lambda_k$  by (6), set  $T_\lambda^\alpha = 0.25T_\lambda$

**output:** ZARU judgment condition  $D_k^\alpha$

- 1: STEP1: get initial detection output  $D_k^\alpha = (\lambda_k < T_\lambda^\alpha)$ , and improve detection results by applying Algorithm 1
  - 2: STEP2: only approve stationary detection results lasting at least 5 s, using method like *STEP2* in Algorithm 1.
- 

3) *Straight-Line Constraint*: When a pedestrian walks along a straight line in an indoor environment, the straight-line constraint algorithm can be used to estimate the heading error, and then improve the accuracy of the Foot-INS [24, 25, 38]. The stride directions of five continuous steps are utilized to detect whether a pedestrian is walking on a straight-line path. The straight-line judgment condition is given as follows:

$$L_1 = \begin{cases} 1, & \max \{|\theta^s - \text{mean}(\theta^s)|\} < T_{1,\theta} \\ 0, & \text{others} \end{cases} \quad (15)$$

$$\begin{cases} \theta^s = \{\theta_{m-4}^s, \theta_{m-3}^s, \dots, \theta_m^s\} \\ \theta_m^s = \text{atan2}(\mathbf{r}_{y,m}^n - \mathbf{r}_{y,m-1}^n, \mathbf{r}_{x,m}^n - \mathbf{r}_{x,m-1}^n) \end{cases} \quad (16)$$

where  $(\mathbf{r}_{x,m}^n, \mathbf{r}_{y,m}^n)$  represents the  $m$ -th step position estimated by the Foot-INS, and the step count needs to satisfy the adjacent step distance  $\Delta d_m = \|(\Delta \mathbf{r}_m^x, \Delta \mathbf{r}_m^y)\| \geq 1.0$ ;  $T_{1,\theta}$  is the direction threshold and is set to  $15^\circ$ . If  $L_1 = 1$ , the pedestrian is walking along a straight line.

Pedestrians can walk along straight lines in the dominant and non-dominant directions. The difference  $\delta\theta_m^s$  between the stride direction  $\theta_m^s$  and the closest building dominant direction is used to determine whether the pedestrian is walking along the dominant direction, and is given as follows:

$$L_2 = \begin{cases} 1, & |\theta_m^s - \theta_b| < T_{2,\theta} \\ 0, & \text{others} \end{cases} \quad (17)$$

$$\theta_b = \arg \min_{\theta_b \in \{0^\circ, 45^\circ, \dots, 315^\circ\}} |\theta_m^s - \hat{\theta}_b| \quad (18)$$

where  $T_{2,\theta}$  is the direction threshold and is set to  $5^\circ$ . If  $L_2 = 1$ , the pedestrian is walking in a straight line along the dominant direction. When a pedestrian is walking along a straight line in the dominant direction of a multistory building, the measurement model is derived as follows:

$$\theta_m^s - \theta_b = \begin{bmatrix} \mathbf{0}_{1 \times 6} & \frac{\partial \psi}{\partial \phi_x} & \frac{\partial \psi}{\partial \phi_y} & \frac{\partial \psi}{\partial \phi_z} & \mathbf{0}_{1 \times 6} \end{bmatrix} \mathbf{X}_k + \varepsilon_\psi \quad (19)$$

where  $\psi$  is the heading angle. The details of  $(\frac{\partial \psi}{\partial \phi_x}, \frac{\partial \psi}{\partial \phi_y}, \frac{\partial \psi}{\partial \phi_z})$  are given in Reference [33]. Noise  $\varepsilon_\psi$  is zero mean white noise given by covariance matrix  $\mathbf{R} = (2^\circ)^2$  [38].

When the pedestrian is not walking in the dominant direction of the multistory building but is walking in a straight line, the measurement model is given as follows:

$$\frac{\theta_m^s - \theta_{m-4}^s}{\Delta t} = [\mathbf{0}_{1 \times 13} \quad \sec \theta \sin \phi \quad \sec \theta \cos \phi] \mathbf{X}_k + \varepsilon_\psi \quad (20)$$

where  $\theta$  and  $\phi$  are the roll and pitch angles estimated by the Foot-INS, respectively.  $\varepsilon_\psi$  is the direction noise, and the corresponding covariance matrix  $\mathbf{R}$  is set to  $(2^\circ)^2$ .

4) *Height Update*: In this study, we focused on pedestrians walking up/downstairs and horizontally. In addition, we assumed that each stair-step height was nearly identical and that multistory buildings do not have any sloping floors or ramps. These assumptions hold for most indoor positioning scenarios in multistory buildings. Therefore, the height difference between two adjacent steps was used to determine whether the pedestrian has walked up/downstairs or horizontally.

The stair-step height of a multistory building can be estimated by Foot-INS when a pedestrian initially ascends the stairs. Then, when the pedestrian is detected walking up/downstairs, the stair-step height can be used as an observation to constrain the height of the Foot-INS in each gait cycle [38, 39]. When the pedestrian chooses to take the elevator to another floor, the Foot-INS floor needs to be manually input.

5) *Closing Point Constraint*: The closing points represent the fire-fighting stair or elevator on each floor of a multistory building. The closing point constraint is the horizontal position constraint and is given as follows:

$$\mathbf{r}_{I,k|1:2}^n - \mathbf{r}_c^n = [\mathbf{I}_{2 \times 2} \quad \mathbf{0}_{2 \times 13}] \mathbf{X}_k + \varepsilon_c \quad (21)$$

where  $\mathbf{r}_{I,k|1:2}^n$  is the horizontal position estimated by the Foot-INS; and the covariance matrix  $\mathbf{R}$  of the observation noise  $\varepsilon_c$  is set to  $\text{diag}[(0.5, 0.5)^2]$ . When a pedestrian initially reaches the closing point on the first floor of a multistory building, the horizontal position calculated by the Foot-INS is the position of the closing point  $\mathbf{r}_c^n$ . Note that the judgment of whether the pedestrian reached the closing point is manually inputted instead of automatically detected.

#### E. Smoothing Algorithm

Acquiring more accurate pedestrian trajectories is beneficial for indoor positioning applications, and the smoothing algorithm can exploit past, current, and future observation information to significantly improve the accuracy and reliability of estimating pedestrian trajectories. For linear and Gaussian systems, the Rauch-Tung-Striebel (RTS) smoother has been

proven to be the optimal smoothing algorithm to implement within the KF framework [37]. Because the Foot-INS was modeled as a linear and Gaussian system, the RTS was used to smooth the pedestrian trajectory, as given by Algorithm 3. Then, we can obtain the smoothed pedestrian trajectory in a multistory building.

---

**Algorithm 3** RTS Smoother
 

---

**input:** state and covariance matrix estimated by KF:  $\hat{\mathbf{X}}_k, \mathbf{P}_k$ ; and predicted state and covariance matrix:  $\hat{\mathbf{X}}_{k+1|k}$  and  $\mathbf{P}_{k+1|k}$   
**output:** smoothed state and covariance matrix:  $\hat{\mathbf{X}}_{s|k}, \mathbf{P}_{s|k}$   
 1: set initial parameters:  $\hat{\mathbf{X}}_{s|N} = \hat{\mathbf{X}}_N, \mathbf{P}_{s|N} = \mathbf{P}_{s|N}$   
 2: **for**  $k = N-1, \dots, 1$  **do**  
 3:  $\mathbf{K}_{s|k} = \mathbf{P}_k \Phi_{k+1,k}^T \mathbf{P}_{k+1|k}^{-1}$   
 4:  $\hat{\mathbf{X}}_{s|k} = \hat{\mathbf{X}}_k + \mathbf{K}_{s|k} (\hat{\mathbf{X}}_{s|k+1} - \hat{\mathbf{X}}_{k+1|k})$   
 5:  $\mathbf{P}_{s|k} = \mathbf{P}_k + \mathbf{K}_{s|k} (\mathbf{P}_{s|k+1} - \mathbf{P}_{k+1|k}) \mathbf{K}_{s|k}^T$   
 6: **end for**

---

#### IV. TRAJECTORY MATCHING ALGORITHM

Although the ZARU and straight-line constraint algorithms are described in Section III. D can estimate the heading error, they are only accidentally triggered occasionally rather than being a regular feature. In fact, some multistory buildings do not exhibit any straight-line pedestrian trajectories at all. Moreover, the closing point constraint method cannot estimate the heading angle in multistory buildings. Even if the actual pedestrian trajectories on different floors are identical, the heading error divergence rotationally offsets the different floors' trajectories estimated by the Foot-INS.

Therefore, we proposed a post-processing trajectory matching algorithm to correct the rotational offset by assuming that pedestrian trajectories could epitomize the multistory building orientation. We modeled the building orientation as a rectangle and then used it to match the different floors' trajectories.

Trajectory matching is used to calculate the rotation angle between different trajectories. We used each footstep position instead of all the epoch positions to reduce the computation time and costs. Moreover, we used the closing points to divide the entire trajectory into several sub-trajectories. We selected stable trajectory segments to improve the reliability of the trajectory matching algorithm. A stable trajectory segment  $\{(x_k, y_k); (x_{k+1}, y_{k+1}); \dots; (x_{k+m}, y_{k+m})\}$  must satisfy the following conditions:

$$\begin{cases} \sum_{i=k}^{m-1} \|(x_{i+1} - x_i, y_{i+1} - y_i)\| \geq \mathbf{T}_{\text{traj}} \\ \max \{\Delta\theta_k, \dots, \Delta\theta_{k+m-1}\} \leq \mathbf{T}_{\theta_{\text{traj}}} \end{cases} \quad (22)$$

where  $\Delta\theta_k = |\theta_{k+1} - \theta_k|$  is the difference between two adjacent steps in the stride direction, and  $\mathbf{T}_{\text{traj}}$  and  $\mathbf{T}_{\theta_{\text{traj}}}$  are the distance and direction thresholds, respectively. A stable trajectory segment is usually smooth without jumps, e.g., a straight path and a curved path. If the length of the trajectory segment is too short, some jumping footstep positions cannot be eliminated, but too long will retain too few effective trajectory segments. Consider the particular application scenario, so we use at least five steps smoothed footstep positions as a trajectory segment (i.e.,  $\mathbf{T}_{\text{traj}} = 5$  m). Moreover, we set  $\mathbf{T}_{\theta_{\text{traj}}}$  to  $15^\circ$  to determine whether the trajectory segment is smooth.

#### A. Orientation Rectangle Fitting

In the data collection of each floor of a multistory building, the tester's walking route needs to cover all the passable areas of a single floor as completely as possible. Therefore, we used the smoothed trajectory obtained on the floor exhibiting the broadest coverage area to fit the building's orientation rectangle. Without loss of generality, the trajectory exhibiting the broadest coverage area was designated as the first trajectory  $\mathbf{S}_1$ , which is defined as follows:

$$\mathbf{S}_1 = \{(x_1, y_1); (x_2, y_2); \dots; (x_{n_1}, y_{n_1})\} \quad (23)$$

The first trajectory exhibits  $n_1$  footstep positions and its geometric center is  $(\bar{x}, \bar{y}) = \text{mean}(\mathbf{S}_1)$ . Orientation rectangle fitting includes the initial principal axis estimation and orientation rectangle optimization. Specifically, we first estimate an orientation rectangle by an initial principal axis, rotate the orientation rectangle, and finally determine the optimal orientation rectangle. Fig. 4 shows an example of an orientation rectangle fitting.

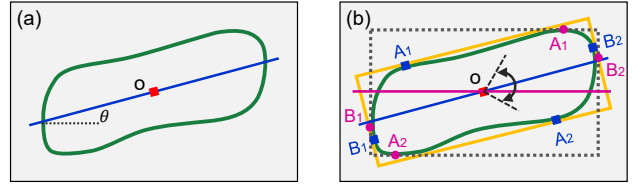


Fig. 4. Orientation rectangle fitting. The green line represents the pedestrian's trajectory. (a) Initial principal axis estimation. (b) Orientation rectangle optimization. Point  $O$  is the geometric center. The yellow box and blue line indicate optimal rectangle and corresponding principal axis, respectively. Purple line and gray dashed box represent rotated principal axis and corresponding rotated orientation rectangle, respectively.

1) *Initial Principal Axis Estimation:* The line passing through the center  $(\bar{x}, \bar{y})$  at angle  $\theta$  is defined as follows:

$$\sin \theta (x - \bar{x}) - \cos \theta (y - \bar{y}) = 0 \quad (24)$$

From the minimum sum of the squared perpendicular distances between the trajectory and the principal axis [40], the angle can be estimated by solving the following optimization problem:

$$\hat{\theta} = \arg \min_{\tilde{\theta}} \mathbf{J}(\tilde{\theta}) \quad (25)$$

$$\mathbf{J}(\tilde{\theta}) = \sum_{i=1}^{n_1} [\sin \tilde{\theta} (x_i - \bar{x}) - \cos \tilde{\theta} (y_i - \bar{y})]^2 \quad (26)$$

The angle estimation is solved by differentiating  $\mathbf{J}(\tilde{\theta})$  with respect to  $\tilde{\theta}$  and setting it to zero. Thus,  $\partial \mathbf{J}(\tilde{\theta}) / \partial \tilde{\theta} = 0$  gives:

$$\tan 2\hat{\theta} = \frac{2 \sum_{i=1}^{n_1} (x_i - \bar{x})(y_i - \bar{y})}{\sum_{i=1}^{n_1} [(x_i - \bar{x})^2 - (y_i - \bar{y})^2]} \quad (27)$$

The possible singularities arising from the solution of (27) must be considered. Then, the two orthogonal central axes of the initial orientation rectangle are given as follows:

$$\begin{cases} \mathbf{f}_1(x, y) = \sin \hat{\theta} (x - \bar{x}) - \cos \hat{\theta} (y - \bar{y}) \\ \mathbf{f}_2(x, y) = \cos \hat{\theta} (x - \bar{x}) + \sin \hat{\theta} (y - \bar{y}) \end{cases} \quad (28)$$

2) *Orientation Rectangle Optimization*: The initial orientation rectangle is essentially the optimal trajectory-line fitting, which is probably not the optimally fitted orientation rectangle. The optimal orientation rectangle must meet the minimum sum of the squared distances from the trajectory. The distance between point  $(x_i, y_i)$  on the pedestrian trajectory and the orientation rectangle (principal axis angle is  $\theta$ ) is defined as follows:

$$d_{\theta,i} = \min \{d_{A_1}^i, d_{A_2}^i, d_{B_1}^i, d_{B_2}^i\} \quad (29)$$

$$\begin{cases} d_{A_j}^i = \|\Delta x_{A_j}^i \sin \theta - \Delta y_{A_j}^i \cos \theta\| \\ d_{B_j}^i = \|\Delta x_{B_j}^i \cos \theta + \Delta y_{B_j}^i \sin \theta\| \end{cases} \quad (30)$$

where  $\Delta x_{A_j}^i = x_i - x_{A_j}$ ,  $\Delta y_{A_j}^i = y_i - y_{A_j}$ , and  $j = 1, 2$ . The pedestrian trajectory can be cut in half by taking a orientation rectangle's central axis as the boundary, and the points farthest from the central axis on both sides are the specific point on the orientation rectangle's edges. The linear equations for the rectangle's four edges can be obtained from (27-28). As shown in Fig. 4,  $A_1$ ,  $A_2$ ,  $B_1$ , and  $B_2$  are the special points on the upper, lower, left, and right edges of the orientation rectangle, respectively. Then, the principle of calculating specific points is given as follows:

$$\begin{cases} (x_{A_1}, y_{A_1}) = \arg \max_{(x_i, y_i) \in S_1} f_1(x_i, y_i) \\ (x_{A_2}, y_{A_2}) = \arg \min_{(x_i, y_i) \in S_1} f_1(x_i, y_i) \\ (x_{B_1}, y_{B_1}) = \arg \min_{(x_i, y_i) \in S_1} f_2(x_i, y_i) \\ (x_{B_2}, y_{B_2}) = \arg \max_{(x_i, y_i) \in S_1} f_2(x_i, y_i) \end{cases} \quad (31)$$

Although estimating the optimally orientated rectangle is basically an optimization problem, it is complex and challenging to solve. Therefore, we rotated the initial orientation rectangle by an optimal angle  $\theta_{\text{opt}}$  around the geometric center to satisfy the following condition:

$$\theta_{\text{opt}} = \arg \min_{\theta \in \mathbf{Z}_\theta} \sum_{i=1}^{n_1} d_{\theta,i}^2 \quad \text{s.t.} \quad \min(\Delta\theta) = 0.1^\circ \quad (32)$$

where  $\mathbf{Z}_\theta = \{(\theta_0 - \theta_1) : \Delta\theta : (\theta_0 + \theta_1)\}$ . Notably, the orientation rectangle was rotated by rotating the four points  $(A_1, A_2, B_1, B_2)$ . The optimal rotation angle was found by conducting three searches. In the first search,  $\theta_0 = \theta_{\text{init}}$ ,  $\theta_{\text{init}}$  was estimated by (27),  $\theta_1 = 45^\circ$ , and  $\Delta\theta = 5^\circ$ . In the second search,  $\theta_0$  was the first optimal rotation angle,  $\theta_1 = \Delta\theta$ , and  $\Delta\theta = 1^\circ$ . In the third search,  $\theta_0$  was the second optimal rotation angle,  $\theta_1 = \Delta\theta$ , and  $\Delta\theta = 0.1^\circ$ . It required 49 iterations to determine the optimally orientation rectangle.

### B. Trajectory Rotation Using Orientation Rectangle

We then matched the pedestrian trajectory and the orientation rectangle with a rotation algorithm using the minimum sum of the squared distances between the trajectory and the orientation rectangle. The closing point was the center of rotation to the other trajectory, and point  $(\tilde{x}_i^j, \tilde{y}_i^j)$  ( $i = 1, \dots, n_j$ ) on the  $j$ th trajectory was rotated by angle  $\alpha$  as follows:

$$\begin{bmatrix} \tilde{x}_i^j \\ \tilde{y}_i^j \end{bmatrix} = \begin{bmatrix} \cos \alpha & -\sin \alpha \\ \sin \alpha & \cos \alpha \end{bmatrix} \begin{bmatrix} x_i^j \\ y_i^j \end{bmatrix} \quad (33)$$

We used threshold  $T_d$  to determine whether the point on the rotated trajectory was available. The distance between that point and the orientation rectangle is defined as follows:

$$\check{d}_i^\alpha = \begin{cases} d_i^\alpha, & d_i^\alpha \leq T_d \\ 0, & d_i^\alpha > T_d \end{cases} \quad (34)$$

where  $d_i^\alpha$  is the minimum distance between the rotated trajectory and the orientation rectangle,  $T_d$  is set to 20 m. The optimal rotation angle  $\alpha_{\text{opt}}$  need satisfy the following conditions:

$$\alpha_{\text{opt}} = \arg \min_{\tilde{\alpha} \in \mathbf{Z}_\alpha} \frac{1}{\tilde{n}_j} \sum (\check{d}_i^{\tilde{\alpha}})^2 \quad (35)$$

$$\text{s.t.} \quad \tilde{n}_j \geq 0.4n_j \quad \text{and} \quad \min(\Delta\alpha) = 0.1^\circ \quad (36)$$

where  $\tilde{n}_j$  is the number of available points on the rotated trajectory and belonging to the set  $\check{d}_i^\alpha > 0$ ,  $\Delta\alpha$  is the set rotation angle spacings, and  $\mathbf{Z}_\alpha^j = \{(\alpha_0 - \alpha_1) : \Delta\alpha : (\alpha_0 + \alpha_1)\}$ . The optimal rotation angle was determined by two searches. Because the rotation difference between the adjacent trajectories arise from the heading divergence of the Foot-INS is less than  $10^\circ$ ,  $\alpha_0 = 0^\circ$ ,  $\alpha_1 = 10^\circ$ , and  $\Delta\alpha = 1^\circ$  in the first search. In the second search,  $\alpha_0$  was the first optimal angle,  $\alpha_1 = \Delta\alpha$ , and  $\Delta\alpha = 0.1^\circ$ . It required 41 iterations to match the pedestrian trajectory and the orientation rectangle.

Fig. 5 shows an example of two trajectories matching. The proposed trajectory matching approach is summarized in Algorithm 4.

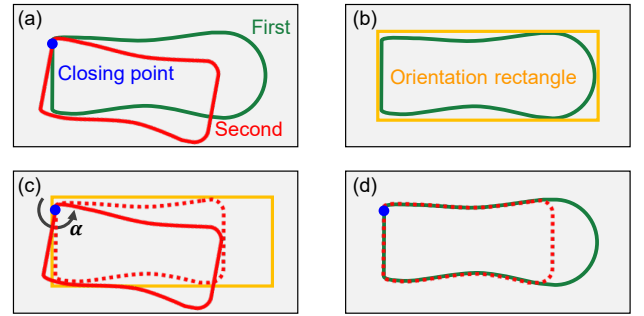


Fig. 5. Example of trajectory matching. (a) Smoothed trajectories. (b) Orientation rectangle fitting. (c) Trajectory matching. (d) Matched trajectories.

---

#### Algorithm 4 Proposed Trajectory Matching Algorithm

---

- input:** smoothed trajectory:  $\{(x_1, y_1); (x_2, y_2); \dots; (x_n, y_n)\}$   
**output:** matched trajectory:  $\{(\hat{x}_1, \hat{y}_1); (\hat{x}_2, \hat{y}_2); \dots; (\hat{x}_m, \hat{y}_m)\}$
- 1: extract each footstep position, and divide whole trajectory into  $q$  segments through closing points.
  - 2: select first trajectory (with broadest coverage area).
  - 3: obtain initial principal axis by (27-28).
  - 4: determine optimally oriented rectangle by (29-32).
  - 5: **for**  $k = 2, \dots, q$  **do**
  - 6:   optimize rotation angle  $\alpha_{\text{opt}}$  between trajectory  $S_k$  and orientation rectangle by (34-36).
  - 7:   rotate trajectory  $S_k$  by (33).
  - 8: **end for**
  - 9: chronologically splice  $q$  rotated trajectories.
-

### C. Trajectory Projection

The pedestrian trajectories obtained by Section IV.B in the different floors of a multistory building are relative. However, the absolute position of pedestrian trajectories in a multistory building is necessary for some practical applications, such as indoor and outdoor seamless navigation and positioning systems. Therefore, we can use two position points with known absolute coordinates to project the pedestrian trajectory into the absolute coordinate frame, which is given as follows:

$$\begin{bmatrix} x_i^a \\ y_i^a \end{bmatrix} = \begin{bmatrix} \cos \alpha_m^a & -\sin \alpha_m^a \\ \sin \alpha_m^a & \cos \alpha_m^a \end{bmatrix} \begin{bmatrix} x_i^m - x_{n1}^m \\ y_i^m - y_{n1}^m \end{bmatrix} + \begin{bmatrix} x_{s1}^a \\ y_{s1}^a \end{bmatrix} \quad (37)$$

$$\alpha_m^a = \arctan(\Delta y^a, \Delta x^a) - \arctan(\Delta y^m, \Delta x^m) \quad (38)$$

where  $(x_i^m, y_i^m)$  is the  $i$ th position on the matched trajectories of different floors in a multistory building,  $(x_i^a, y_i^a)$  is the absolute position.  $\Delta x^a = x_{s2}^a - x_{s1}^a$  is the position difference of two absolute points in the  $x$  direction, and  $\Delta y^a$  is the position difference in the  $y$  direction.  $(\Delta x^m, \Delta y^m)$  is the position difference between the points on the matched trajectory corresponding to the two absolute position points.  $(x_{n1}^m, y_{n1}^m)$  is the point on the matched trajectories corresponding to the first absolute point  $(x_{s1}^a, y_{s1}^a)$ . Noted that in practical applications, the two absolute position points can be selected to be located at the entrance and exit of the buildings, and the absolute position can be measured by the GNSS technique or other professional measurement instruments (e.g., a total station).

## V. EXPERIMENTAL RESULTS

### A. Hybrid Simulation Experiments

We conducted an experimental test in an open area with dimensions of approximately  $80 \times 40$  m ( $3200$  m<sup>2</sup>) to assess the positioning accuracy of the proposed IPPS. As shown in Fig. 6, we planned a walking path to mimic the shape of the trajectory that could be encountered in practical applications. The planned path was divided into four sub-trajectories by the closing point. The second sub-trajectory was the same as the first, and part of the third and fourth sub-trajectories overlapped with the first. An inertial module (described in Table I) was tightly fixed on the heel of a tester's shoe.

The tester started at the closing point, immediately walked four sub-trajectories along the planned path, and finally returned to the closing point. Note that the experimental test was continuous walking rather than separated according to different sub-trajectories. The total length of the test path was about 700 m, of which the lengths of the first, second, third, and fourth sub-trajectories were approximately 190 m, 190 m, 140 m, and 180 m, respectively. The test time was approximately 1250 s.

As shown in Fig. 6, the planned walking path consisted of a series of reference points, which coordinates were measured using a Leica manual total station, and the accuracy was above 5 mm. A corresponding circular mark was then posted directly above each reference point, and the tester walked following the path indicated by the circular marks. When the tester stepped on the mark, the inertia module recorded the identifier sent by the smartphone application. The identifiers facilitated the subsequent accuracy assessment. Because misalignment between

the shoe and the circular mark may cause an additional error of  $1 \sim 3$  cm, the accuracy of the actual reference truth was better than 5 cm.

In order to evaluate the performance of the proposed system, we used two absolute position points with known coordinates to project the matched trajectory into the coordinate frame formed by the reference points. The two absolute position points correspond to the first sub-trajectory.

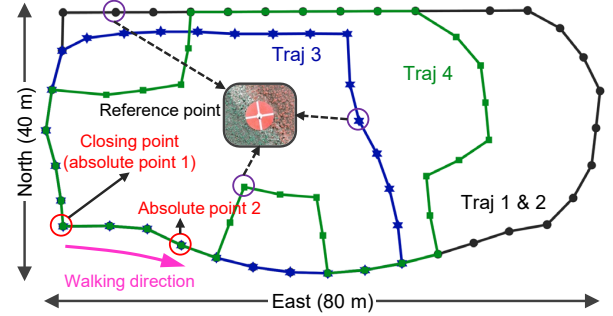


Fig. 6. Planned walking path used for hybrid simulation experiment test.

In the experimental tests, we compared the performances of the Foot-INS with no closing point (FINS), Foot-INS with closing point (FINS/CP), Foot-INS and RTS smoothing (FINS/RTS—as described in Section III), and our proposed IPPS. Moreover, we quantitatively analyzed the positioning accuracy of these methods by calculating the root mean square (RMS), maximum (MAX), and cumulative distribution function (CDF) of the horizontal positioning error  $\varepsilon$ , which is defined as follows:

$$\varepsilon = \sqrt{(\mathbf{r}_{\text{est}}^n - \mathbf{r}_{\text{ref}}^n)^2 + (\mathbf{r}_{\text{est}}^e - \mathbf{r}_{\text{ref}}^e)^2} \quad (39)$$

where  $(\mathbf{r}_{\text{est}}^n, \mathbf{r}_{\text{est}}^e)$  is the horizontal position estimated using the different approaches, and  $(\mathbf{r}_{\text{ref}}^n, \mathbf{r}_{\text{ref}}^e)$  is the reference position.

Fig. 7 compares the position trajectories estimated using the four different methods. The horizontal positioning error estimated by the four different approaches is shown in Fig. 8, and Fig. 9 exhibits the CDF of the positioning error. Furthermore, we statistically analyzed the RMS and MAX of the horizontal positioning errors obtained using the four different methods in the hybrid simulation experiment, and the results are listed in Table II.

TABLE II  
POSITIONING ERROR STATISTICS OBTAINED USING DIFFERENT METHODS  
IN HYBRID SIMULATION EXPERIMENT.

| Position error (m) | FINS    | FINS/CP | FINS/RTS | Proposed |      |
|--------------------|---------|---------|----------|----------|------|
| RMS                | Traj 1  | 3.48    | 3.48     | 0.45     | 0.45 |
|                    | Traj 2  | 3.49    | 3.08     | 1.85     | 0.59 |
|                    | Traj 3  | 4.08    | 2.69     | 2.90     | 1.06 |
|                    | Traj 4  | 6.95    | 6.83     | 6.14     | 1.28 |
|                    | Average | 4.50    | 4.02     | 2.84     | 0.85 |
| MAX                | Traj 1  | 6.25    | 6.25     | 0.82     | 0.82 |
|                    | Traj 2  | 6.16    | 4.59     | 3.52     | 1.00 |
|                    | Traj 3  | 6.10    | 5.07     | 4.29     | 1.69 |
|                    | Traj 4  | 10.94   | 10.51    | 10.43    | 2.19 |

Fig. 7 clearly shows that many curves in the planned walking path, ZARU and the straight-line constraint algorithms cannot

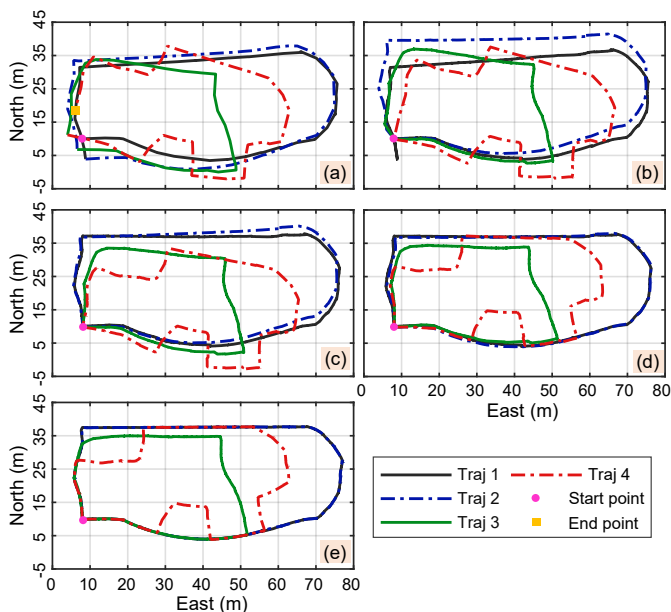


Fig. 7. Estimated trajectories using different methods in the hybrid simulation experiment. (a) FINS, (b) FINS/CP, (c) FINS/RTS, (d) Proposed, and (e) Reference. In (b-e), the start and end points of four sub-trajectory are coincident and located at the closing point.

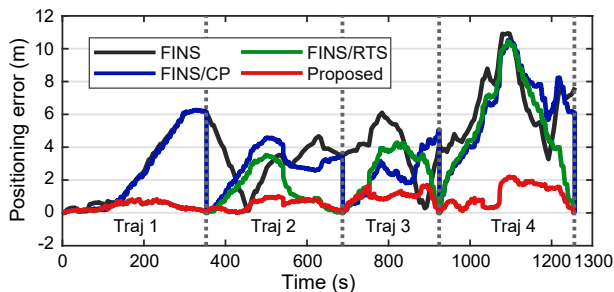


Fig. 8. Horizontal positioning error obtained from four different methods in the hybrid simulation experiment.

effectively estimate the heading angle, leading to the position error estimated by FINS still diverges continuously. Since the experimental test is continuous and uninterrupted, each sub-trajectories obtained from the FINS method cannot be closed and has a rotation deviation error between the four different sub-trajectories. In the FINS/CP method, the closing point can be used as a constraint to improve the positioning accuracy at the beginning and end of the different sub-trajectories, so the start point of each sub-trajectory is located at the closing point. However, the FINS/CP method cannot estimate the heading error due to the lack of adequate observation information. When the difference between the estimated and the corresponding covariance matrix of FINS/CP at two closing points (i.e., the beginning and end of each trajectory) is very close, the RTS smoothing algorithm could not improve the positioning accuracy. Similarly, FINS/RTS could not prevent the divergence of the heading angle. The proposed IPPS could match the second to fourth sub-trajectories with the first one, which effectively improved the estimation accuracy of the pedestrian trajectory. The average position estimation

accuracy (RMS) of the proposed IPPS for the different sub-trajectories was 0.85 m. Compared with the FINS, FINS/CP, and FINS/RTS approaches, the proposed method could improve the positioning accuracy (RMS) by 81%, 79%, and 70%, respectively.

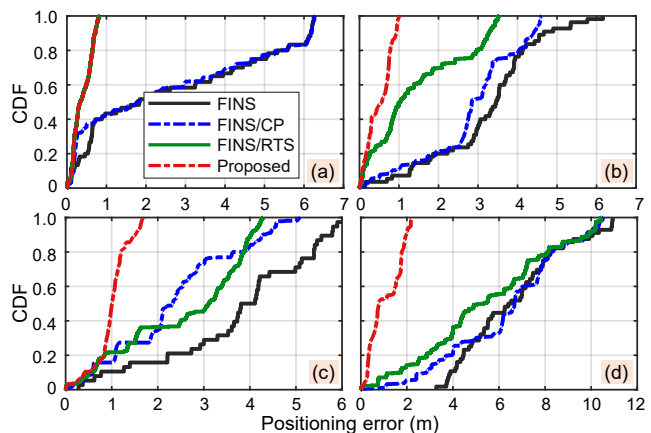


Fig. 9. CDF of horizontal positioning error using four different methods in the hybrid simulation experiment. (a) First, (b) second, (c) third, and (d) fourth sub-trajectories.

## B. Shopping Mall Experiments

To test the effectiveness of the proposed IPPS in practical applications and determine whether this approach has a practical value, we conducted several experimental tests in a large shopping mall in the Wuhan Yintai Creative City. The shopping mall is a typical ten-floor multistory indoor building that integrates shopping, entertainment, leisure, and dining facilities. Fig. 10 shows some experimental test environments in the mall.



Fig. 10. Test environments used for shopping mall experiments. (a) Fire-fighting stair. (b) Corridor. (c) Third floor. (d) Fifth floor.

In particular, we projected the positioning trajectory obtained from four different methods onto a public map platform in the shopping mall experimental tests. Since the shopping mall map was inaccurate, we zoomed and corrected the map using four points with accurate absolute positions. Any information from the shopping mall map was not used to assist the proposed system, the map was only used as a visual tool to clearly illustrate the walking path in the experimental tests. Moreover, the two absolute position points with known coordinates were used to align the matched trajectory with the corrected shopping mall map.

1) *Repeated Circular Paths*: We first conducted an experimental test using repeated circular paths on the 6th floor of the shopping mall. The tester walked five times repeatedly along a path about 2 m away from the outermost store. The experimental test was continuous walking rather than separated

according to different sub-trajectories. The total length of the test path was about 1500 m, and each sub-trajectories lengths were approximately 300 m. The test time was approximately 1270 s. The FINS, FINS/CP, FINS/RTS, and proposed IPPS methods were employed to estimate the pedestrian trajectories, and the results are shown in Fig. 11.

The five circular sub-trajectories were repeated, and the first sub-trajectory estimated using FINS/RTS was identical to the one estimated using the proposed IPPS. Therefore, we used the first FINS/RTS sub-trajectory as the reference in the repeated circular path experiments. We using the repeatability error to evaluate the positioning accuracy of the different methods. The repeatability error was defined as the distance between each of the five trajectories and the reference. Fig. 12 shows the trajectory repeatability error obtained for the four different methods. Moreover, the repeatability error statistics obtained using four different approaches are listed in Table III.

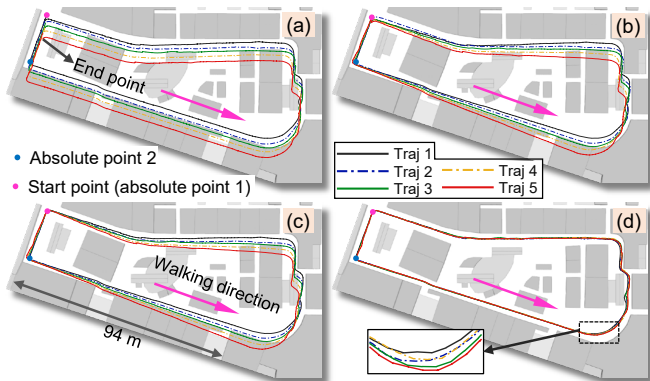


Fig. 11. Position trajectories obtained from (a) FINS, (b) FINS/CP, (c) FINS/RTS, and (d) proposed IPPS methods in repeated circular path experiments conducted in the shopping mall. The two absolute position points correspond to the first sub-trajectory, and the purple arrow represents the walking direction.

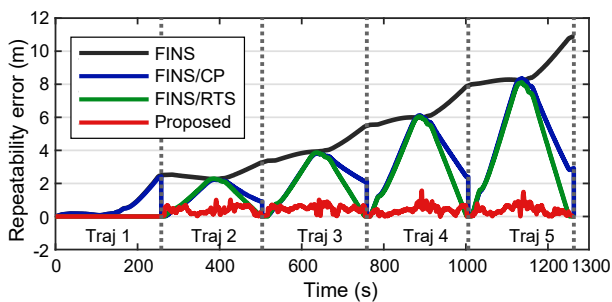


Fig. 12. Repeatability error obtained using different methods in repeated circular path experiments conducted in the shopping mall.

Since the walking path of the repeated circular trajectory experiments includes some curve segments, the straight-line constraint algorithm is not always effective. Each sub-trajectory obtained by the FINS method for continuous positioning estimation cannot be closed, and its position error increases with time. Both FINS/CP and FINS/RTS methods cannot reliably estimate the heading angle only rely on the closing point, resulting in a rotation deviation between the five sub-trajectories. The proposed IPPS significantly improved the

estimation accuracy of the pedestrian trajectory. The repeatability error (RMS) of the proposed method was below 0.5 m, and the MAX was approximately 1.5 m. Compared to the repeatability of the estimation accuracy obtained using the FINS/RTS algorithm, that of the proposed IPPS on the second to fifth sub-trajectories had improved by 68 %, 78 %, 88 %, and 91 %, respectively.

TABLE III  
REPEATABILITY ERROR STATISTICS OF DIFFERENT METHODS IN REPEATED CIRCULAR TRAJECTORY EXPERIMENTS CONDUCTED IN SHOPPING MALL.

| Repeatability error | FINS   | FINS/CP | FINS/RTS | Proposed |      |
|---------------------|--------|---------|----------|----------|------|
| RMS (m)             | Traj 1 | 0.96    | 0.93     | 0        | 0    |
|                     | Traj 2 | 2.56    | 1.41     | 1.33     | 0.42 |
|                     | Traj 3 | 4.09    | 2.45     | 2.15     | 0.48 |
|                     | Traj 4 | 6.29    | 3.86     | 3.47     | 0.42 |
|                     | Traj 5 | 8.98    | 5.02     | 4.44     | 0.41 |
| MAX (m)             | Traj 1 | 2.50    | 2.50     | 0        | 0    |
|                     | Traj 2 | 3.27    | 2.23     | 2.20     | 1.01 |
|                     | Traj 3 | 5.48    | 3.81     | 3.76     | 1.01 |
|                     | Traj 4 | 7.91    | 6.11     | 6.05     | 1.56 |
|                     | Traj 5 | 10.91   | 8.36     | 8.11     | 1.48 |

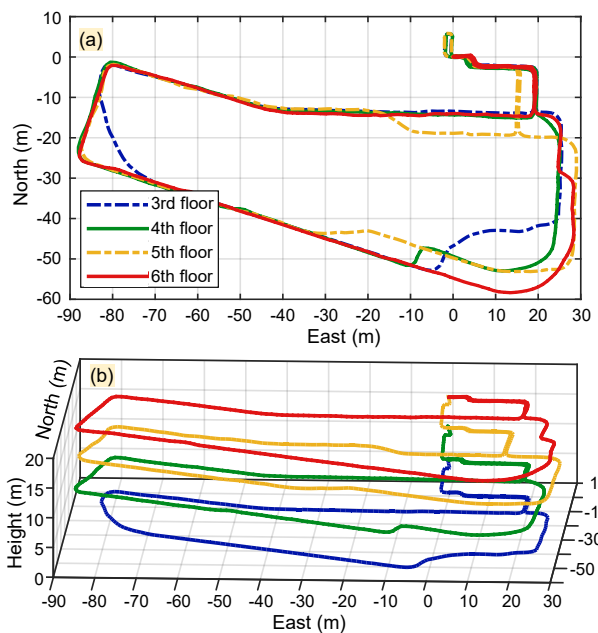


Fig. 13. Positioning trajectories estimated using proposed IPPS in shopping mall multi-floor test. (a) horizontal and (b) three-dimensional results.

2) *Multi-Floor Test*: We also conducted a multi-floor experiment test on the third to sixth floors of the shopping mall. The fire-fighting stair shown in Fig. 10 (a) was selected as the shopping mall closing point, and its horizontal position is identical on each floor. The tester walked from the third to the sixth floor of the shopping mall. They started from the closing point, walked around the core area, returned to the starting point on each floor, and then went upstairs to continue data collection on the next floor until the end. The test was continuous walking mode rather than separated according to different floors. The total length of the test path was about 1450 m, and the lengths of the walking paths on the third to

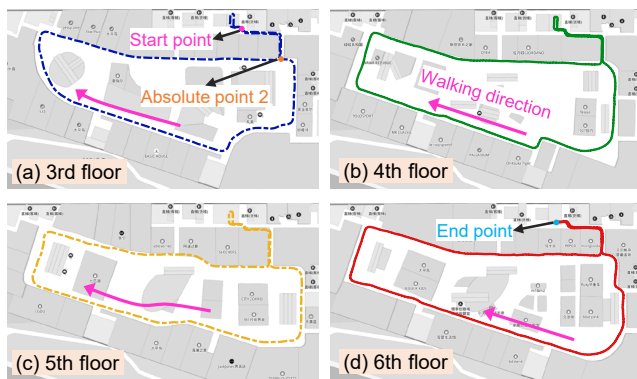


Fig. 14. Different horizontal floor positions obtained by proposed IPPS projected onto a corrected map platform in shopping mall multi-floor test. The two absolute points ('Start point' and 'Absolute point 2') in (a) were located on the third floor and used to align the matched trajectory with the corrected shopping mall map.

the sixth floors were approximately 350 m, 370 m, 370 m, and 360 m, respectively. The test time was approximately 1450 s. The core area and the closing point (i.e., fire-fighting stair) are separated by a corridor, as shown in Fig. 10 (b), each floor's corridor is different in the horizontal projection.

Fig. 13 shows the pedestrian trajectories obtained using the proposed IPPS. The different floor sub-trajectories were projected on a corrected shopping mall map in Fig. 14. The results show that the proposed IPPS can effectively estimate the positioning trajectory of the pedestrian, and the estimated sub-trajectory of different floors is basically consistent with the actual walking path.

Shopping malls are an environment wherein people have the most imperious demand for ILBS. The results of the various shopping mall experimental tests validated the effectiveness of the proposed IPPS, and also demonstrated the potential and value of the proposed method in practical applications.

## VI. CONCLUSIONS AND FUTURE WORK

We have presented an accurate and convenient Foot-INS based indoor pedestrian positioning system (IPPS) in post-processing mode, so as to estimate the pedestrian trajectories in unmapped multistory buildings such as shopping malls. Foot-INS (including the ZUPT, ZARU, straight-line constraint, and height update algorithms) is the basis of the proposed IPPS. The fire-fighting stairs or elevators of a multistory building were selected as the closing point of the proposed IPPS. Because the horizontal position of the closing point was almost identical on each floor, the closing point was used to constrain the trajectory drift error caused by the Foot-INS on a single floor. A smoothing algorithm is applied to reasonably distribute the drift error to the entire trajectory. Based on the hypothesis that the pedestrian trajectory could epitomize the building orientation. We also proposed a trajectory matching algorithm in post-processing mode, to mitigate the rotational offset due to the unavoidable heading divergence between the different floor trajectories. The hybrid simulation experiment results revealed that the positioning trajectory RMS error of the proposed IPPS was 0.85 m and that the IPPS improved

the positional accuracy by 81% compared to the Foot-INS. The results of the repeated circular trajectory experiments conducted in the shopping mall showed that the trajectory repeatability RMS error of the proposed IPPS was below 0.5 m. Moreover, the multi-floor experiment conducted in a large shopping mall demonstrated the effectiveness and practical application potential of the proposed IPPS.

Furthermore, the proposed IPPS shows good potential for large-scale promotion because testers do not require a professional background, and the building does not have to be measured in advance. We are currently collaborating with the industry to explore the feasibility of applying the proposed IPPS to establish the WiFi fingerprint database of shopping malls in major cities in China. In the future, we plan to dig deeper into the more useful structural characteristics of buildings to improve the reliability of the Foot-INS. We will also enhance the trajectory matching algorithm to adapt to more complex and diverse multistory indoor buildings. Moreover, we are exploring the use of multistory building structural characteristics to develop a real-time IPPS.

## REFERENCES

- [1] Markets and Markets, "Indoor location market by component (hardware, solutions, and services), deployment mode, organization size, technology, application, vertical (retail, transportation and logistics, entertainment), and region-global forecast to 2025," <https://www.marketsandmarkets.com/Market-Reports/indoor-location-market-989.html>, May, 2020.
- [2] H. Zou, M. Jin, H. Jiang, L. Xie, and C. J. Spanos, "Winips: Wifi-based non-intrusive indoor positioning system with online radio map construction and adaptation," *IEEE Trans. Wireless Commun.*, vol. 16, no. 12, pp. 8118–8130, 2017.
- [3] G. Caso, L. De Nardis, F. Lemic, V. Handziski, A. Wolisz, and M. D. Benedetto, "Vifi: Virtual fingerprinting wifi-based indoor positioning via multi-wall multi-floor propagation model," *IEEE Trans. Mobile Comput.*, vol. 19, no. 6, pp. 1478–1491, 2020.
- [4] R. Faragher and R. Harle, "Location fingerprinting with bluetooth low energy beacons," *IEEE J. Sel. Areas Commun.*, vol. 33, no. 11, pp. 2418–2428, 2015.
- [5] S. Fang, C. Wang, T. Huang, C. Yang, and Y. Chen, "An enhanced zigbee indoor positioning system with an ensemble approach," *IEEE Commun. Lett.*, vol. 16, no. 4, pp. 564–567, 2012.
- [6] J. Zhang, Y. Lyu, J. Patton, S. C. G. Periaswamy, and T. Roppel, "Bfvp: A probabilistic uhf rfid tag localization algorithm using bayesian filter and a variable power rfid model," *IEEE Trans. Ind. Electron.*, vol. 65, no. 10, pp. 8250–8259, 2018.
- [7] T. Liu, X. Niu, J. Kuang, S. Cao, L. Zhang, and X. Chen, "Doppler shift mitigation in acoustic positioning based on pedestrian dead reckoning for smartphone," *IEEE Trans. Instrum. Meas.*, vol. 70, pp. 1–11, 2021.
- [8] G. De Angelis, A. Moschitta, and P. Carbone, "Positioning techniques in indoor environments based on stochastic modeling of ubw round-trip-time measurements," *IEEE Trans. Intell. Transp. Syst.*, vol. 17, no. 8, pp. 2272–2281, 2016.
- [9] H. Xie, T. Gu, X. Tao, H. Ye, and J. Lu, "A reliability-augmented particle filter for magnetic fingerprinting based indoor localization on smartphone," *IEEE Trans. Mobile Comput.*, vol. 15, no. 8, pp. 1877–1892, 2016.
- [10] J. Kuang, X. Niu, P. Zhang, and X. Chen, "Indoor positioning based on pedestrian dead reckoning and magnetic field matching for smartphones," *Sensors*, vol. 18, no. 12, 2018.
- [11] R. Mur-Artal and J. D. Tardós, "Orb-slam2: An open-source slam system for monocular, stereo, and rgb-d cameras," *IEEE Trans. Robot.*, vol. 33, no. 5, pp. 1255–1262, 2017.

- [12] D. Droschel, M. Schwarz, and S. Behnke, "Continuous mapping and localization for autonomous navigation in rough terrain using a 3d laser scanner," *Robot. Auton. Syst.*, vol. 88, pp. 104–115, 2017.
- [13] A. R. Jiménez, F. Seco, J. C. Prieto, and J. Guevara, "Indoor pedestrian navigation using an ins/ekf framework for yaw drift reduction and a foot-mounted imu," in *Proc. 7th Workshop Positioning, Navig. Commun.*, Mar. 2010, pp. 135–143.
- [14] J. Bird and D. Arden, "Indoor navigation with foot-mounted strapdown inertial navigation and magnetic sensors," *IEEE Wireless Commun.*, vol. 18, no. 2, pp. 28–35, 2011.
- [15] S. Qiu, Z. Wang, H. Zhao, K. Qin, Z. Li, and H. Hu, "Inertial/magnetic sensors based pedestrian dead reckoning by means of multi-sensor fusion," *Inf. Fusion*, vol. 39, pp. 108–119, 2018.
- [16] L. Shi, Y. Zhao, G. Liu, S. Chen, Y. Wang, and Y. Shi, "A robust pedestrian dead reckoning system using low-cost magnetic and inertial sensors," *IEEE Trans. Instrum. Meas.*, vol. 68, no. 8, pp. 2996–3003, 2019.
- [17] C. M. N. Brigante, N. Abbate, A. Basile, A. C. Faulisi, and S. Sessa, "Towards miniaturization of a mems-based wearable motion capture system," *IEEE Trans. Ind. Electron.*, vol. 58, no. 8, pp. 3234–3241, 2011.
- [18] N. Yu, Y. Li, X. Ma, Y. Wu, and R. Feng, "Comparison of pedestrian tracking methods based on foot- and waist-mounted inertial sensors and handheld smartphones," *IEEE Sensors J.*, vol. 19, no. 18, pp. 8160–8173, 2019.
- [19] R. Harle, "A survey of indoor inertial positioning systems for pedestrians," *IEEE Commun. Surveys Tuts.*, vol. 15, no. 3, pp. 1281–1293, 2013.
- [20] N. El-Sheimy and Y. Li, "Indoor navigation: state of the art and future trends," *Satell. Navigat.*, vol. 1, no. 2, p. 7, 2021.
- [21] E. Foxlin, "Pedestrian tracking with shoe-mounted inertial sensors," *IEEE Comput. Graph. Appl.*, vol. 25, no. 6, pp. 38–46, 2005.
- [22] A. Ramanandan, A. Chen, and J. A. Farrell, "Inertial navigation aiding by stationary updates," *IEEE Trans. Intell. Transp. Syst.*, vol. 13, no. 1, pp. 235–248, 2012.
- [23] Y. Wang, A. Chernyshoff, and A. M. Shkel, "Study on estimation errors in zupt-aided pedestrian inertial navigation due to imu noises," *IEEE Trans. Aerosp. Electron. Syst.*, vol. 56, no. 3, pp. 2280–2291, 2020.
- [24] J. Borenstein and L. Ojeda, "Heuristic drift elimination for personnel tracking systems," *J. Navig.*, vol. 63, no. 4, p. 591, 2010.
- [25] A. R. Jiménez, F. Seco, F. Zampella, J. C. Prieto, and J. Guevara, "Improved heuristic drift elimination (ihde) for pedestrian navigation in complex buildings," in *Proc. Int. Conf. Indoor Position. Indoor Navig.*, Sep. 2011, pp. 1–8.
- [26] Z. Deng, P. Wang, T. Liu, Y. Cao, and B. Wang, "Foot-mounted pedestrian navigation algorithm based on bor/mins integrated framework," *IEEE Trans. Ind. Electron.*, vol. 67, no. 5, pp. 3980–3989, 2020.
- [27] X. Niu, T. Liu, J. Kuang, and Y. Li, "A novel position and orientation system for pedestrian indoor mobile mapping system," *IEEE Sensors J.*, vol. 21, no. 2, pp. 2104–2114, 2021.
- [28] T. Liu, J. Kuang, W. Ge, P. Zhang, and X. Niu, "A simple positioning system for large-scale indoor patrol inspection using foot-mounted ins, qr code control points, and smartphone," *IEEE Sensors J.*, vol. 21, no. 4, pp. 4938–4948, 2021.
- [29] S. Beauregard and M. Klepal, "Indoor pdr performance enhancement using minimal map information and particle filters," in *Proc. IEEE Location Navig. Symp.*, 2008, pp. 141–147.
- [30] A. Perttula, H. Leppäkoski, M. Kirkko-Jaakkola, P. Davidson, J. Collin, and J. Takala, "Distributed indoor positioning system with inertial measurements and map matching," *IEEE Trans. Instrum. Meas.*, vol. 63, no. 11, pp. 2682–2695, 2014.
- [31] H. Xia, J. Zuo, S. Liu, and Y. Qiao, "Indoor localization on smartphones using built-in sensors and map constraints," *IEEE Trans. Instrum. Meas.*, vol. 68, no. 4, pp. 1189–1198, 2019.
- [32] Z. Han, W. Weng, Q. Zhao, X. Ma, Q. Liu, and Q. Huang, "Investigation on an integrated evacuation route planning method based on real-time data acquisition for high-rise building fire," *IEEE Trans. Intell. Transp. Syst.*, vol. 14, no. 2, pp. 782–795, 2013.
- [33] E.-H. Shin, "Estimation techniques for low-cost inertial navigation," Ph.D. dissertation, Dept. Geomatics Eng., Univ. Calgary, Calgary, AB, Canada, 2005.
- [34] J. Kuang, X. Niu, and X. Chen, "Robust pedestrian dead reckoning based on mems-imu for smartphones," *Sensors*, vol. 18, no. 5, 2018.
- [35] I. Skog, P. Handel, J. Nilsson, and J. Rantakokko, "Zero-velocity detection—an algorithm evaluation," *IEEE Trans. Biomed. Eng.*, vol. 57, no. 11, pp. 2657–2666, 2010.
- [36] Z. Wang, H. Zhao, S. Qiu, and Q. Gao, "Stance-phase detection for zupt-aided foot-mounted pedestrian navigation system," *IEEE/ASME Trans. Mechatronics*, vol. 20, no. 6, pp. 3170–3181, 2015.
- [37] R. G. Brown and P. Y. C. Hwang, *Introduction to random signals and applied Kalman filtering: with MATLAB exercises, 4th ed.* Hoboken, NJ, USA: John Wiley & Sons, 2012.
- [38] K. Abdulrahim, C. Hide, T. Moore, and C. Hill, "Using constraints for shoe mounted indoor pedestrian navigation," *J. Navig.*, vol. 65, no. 1, pp. 15–28, 2012.
- [39] N. Bai, Y. Tian, Y. Liu, Z. Yuan, Z. Xiao, and J. Zhou, "A high-precision and low-cost imu-based indoor pedestrian positioning technique," *IEEE Sensors J.*, vol. 20, no. 12, pp. 6716–6726, 2020.
- [40] D. Chaudhuri and A. Samal, "A simple method for fitting of bounding rectangle to closed regions," *Pattern Recognit.*, vol. 40, no. 7, pp. 1981–1989, 2007.



**Xiaoji Niu** received the B.Eng. degree (with honors) in Mechanical and Electrical Engineering and the Ph.D. from Tsinghua University, Beijing, China, in 1997 and 2002, respectively. From 2003 to 2007, he was a Post-Doctoral Fellow with the Mobile MultiSensor Systems (MMSS) Research Group, Department of Geomatics Engineering, and University of Calgary. From 2007 to 2009, he was a Senior Scientist with SiRF Technology, Inc. At present, he is a Professor of the GNSS Research Center and the Collaborative Innovation Center of Geospatial

Technology in Wuhan University, Wuhan, China. His research interests focus on INS, GNSS/INS integration for land vehicle navigation and pedestrian navigation.



**Tao Liu** received the B.S. degree in Geographic Information System from Liaoning Technical University, Fuxin, China, in 2015, and M.S. degree in Surveying and Mapping from Liaoning Technical University, Fuxin, China, in 2018. He is currently pursuing the Ph.D. degree in GNSS Research Center, Wuhan University, Wuhan, China. His research interests focus on inertial navigation, multi-sensor fusion algorithm, IMU-based body sensor network, pedestrian navigation and indoor positioning.



**Jian Kuang** received the B.Eng. degree and Ph.D. degree in Geodesy and Survey Engineering from Wuhan University, Wuhan, China, in 2013 and 2019, respectively. He is currently a Postdoctoral Fellow with the GNSS Research Center in Wuhan University, Wuhan, China. His research interests focus on inertial navigation, pedestrian navigation and indoor positioning.



**Quan Zhang** (Member, IEEE) received the B.S. degree in geomatics engineering from the Shandong University of Science and Technology in 2009 and the Ph.D. degree from Wuhan University in 2015. From 2017 to 2018, he was a Post-Doctoral Researcher with the Digital Photogrammetry Research Group (DPRG), Lyles School of Civil Engineering, Purdue University. He is currently a Research Assistant and a Post Doctor with the GNSS Research Center and the Collaborative Innovation Center of Geospatial Technology, Wuhan University. His research interests include

the inertial navigation and the GPS/INS integration technology.



**Chi Guo** (Member, IEEE) received the M.Eng. and Ph.D. degrees in computer science from Wuhan University, Wuhan, China. He is currently a Professor with the GNSS Research Center and the Artificial Intelligence Institute in Wuhan University, Wuhan, China. His research interests include BeiDou application, unmanned system navigation, and location-based services (LBS).